A Graphene-Based Aerogel Was Prepared as Solid Adsorbent for the Enrichment of Platinum (IV) at Trace Concentration

Lei Chen[1,2], Han Diao[2], Qijiang Shu[3*], Tao Yang[4*]

[1]Faculty of Narcotics Control, Yunnan Police College, Kunming, China
[2]College of Chinese Materia Medicine, Yunnan University of Chinese Medicine, Kunming, China
[3]Institute of Information, Yunnan University of Chinese Medicine, Kunming, China
[4]Administration Office of Scientific Research, Yunnan Institute of Tropical Crops, Jinghong, China
Email: *sqj22yjy@163.com, *ericyang1112@163.com

Abstract

A three-dimensional graphene-based composite was prepared by a simple one-step in-site reduced-oxide method under atmospheric pressure. The obtained hydrogel was modified with 4-amino-benzenesulfonic acid and connected with ethylenediamine, and freeze-dried into an aerogel, which was characterized. Then the surface interaction with platinum (Pt, IV) was explored. The obtained aerogel showed good adsorption for Pt (IV) at acid conditions, giving a rising to the adsorption rate > 98% while pH ≥ 6. Using hexadecyl trimethyl ammonium bromide of 2% (m/V) as an eluent to desorb the Pt (IV) from the surface of the aerogel, a desorption rate of 81.1% was obtained in this process. Urea, buffer aquation and other surfactants were used in the desorption experiment to understand the adsorption mechanism between the aerogel and Pt (IV). In this work, hydrogen bond, van der Waals force and electronic interaction force mainly drove the adsorption process. For obtaining more purified Pt (IV), we used 0.5% CTAB to desorb Pd (II). A new three-dimensional graphene-based composite was prepared and the surface interaction between Pt (IV) and composite was experimented for understanding the adsorption mechanism and exploring its potential application in sample preparation in low concentration.

Keywords

Graphene, Platinum (IV), Aerogel, Sample Preparation, Three-Dimensional

1. Introduction

Platinum was confirmed by British chemist Watson in 1748. Pt has good wear

and tarnishes resistance characteristics, which is well suited for making fine jewelry. Besides, its chemical property is extremely stable, excellent high-temperature, rich charge-transfer transitions, face-centered cubic and shows a strong characteristic of absorbing gas, such as H_2 [1] [2]. Therefore, it attracted researchers' interest to widely exploit it for industrial applications, such as catalyst [3] [4] [5] [6] [7], including the chemical industry, petroleum industry and automobile catalyst et al, electronic components [8] [9] [10] [11], chemical and biological sensors [12] [13] [14], anticancer drugs [15] [16] [17] [18] and luminescent platinum complex probe [19] [20] [21] [22]. As the global platinum reserves are very limited, the output of main producing countries continue to decline. World resources of platinum-group metals (PGMs) are estimated to totally more than 100 million kilograms, about 115,000 kilograms of palladium and platinum were recovered globally from new and old scrap in 2021, including about 53,000 kilograms recovered from automobile catalytic converters in the United States [23]. China mainly imported platinum from South Africa and Russia to meet the requirement because of the fewer reserves. Platinum and palladium both have high density, high melting point and boiling point, resulting in difficulty to separate and purify, multistage extraction and multiple organic extractants are usually needed. Solid extraction appeared to improve the enrichment ratio, decrease environmental pollution, save time and meet the requirements of the recovery of trace and microscale substances. Graphene oxide (GO) has a honeycomb-like six-ring structure and oxygen-containing groups, making it modified easily in the preparation process. It is a precursor to other graphene-based materials including two-dimensional (2D) and three-dimensional (3D) structure [24] [25] [26] [27]. Graphene-based materials as solid extractants have a big potential to be applied in sample pretreatment by functionalizing graphene oxide, due to the intrinsic biocompatibility, enlarged adsorption capacity, increscent specific surface area and the obtained selective specificity. There were a few papers that reported the enrichment of Pt (IV) in low concentrations by solid extraction. In this work, the new 3D graphene-based aerogel was prepared, and we used it to adsorb 80.0 μg·mL^{-1} Pt (IV) to exploit a new method of recycling Pt (IV) in trace concentration from recycling solution.

2. Materials and Methods

2.1. Materials and Reagents

Urea, hexadecyl trimethyl ammonium bromide (CTAB), 4-amino-benzenesulfonic acid, sodium dodecyl sulfate (SDS), tetrabutylammonium bromide (TBAB), ethylenediamine (EDA), platinum (IV) chloride and palladium (II) chloride were purchased from Aladdin Chemistry Co., Ltd. (Shanghai, China). 0.04 M phosphoric acid, boric acid and acetic acid were mixed, and pH was adjusted by using 0.2 mol·L^{-1} NaOH for preparing Britton-Robinson (B-R) buffer. The other reagents were purchased from Sinopharm Chemical Reagent Co., Ltd. (Shanghai, China). And all the reagents employed were analytical reagent grade unless stated otherwise. Deionized water was used in the whole experiment process.

2.2. Preparation of the Three-Dimensional Graphene-Based Aerogel

GO was prepared by oxidizing and peeling graphene powders by using strongly oxidizing reagents, such as potassium permanganate, hydrogen peroxide, concentrated sulfuric acid et al, according to improved Hummers' method by Chen [28]. GO aqueous suspension was obtained by adding 50 mg GO into 100 mL deionized water, then sonicating for a few hours till GO dispersed evenly in the solution. 5 mL 4-amino-benzenesulfonic acid of 20 mg·mL^{-1} was mixed with 5 mL GO suspension, the mixture was sealed and put into a water bath without stirring at 90°C for 7 h under the atmosphere temperature. Before the heating process, 100 μL EDA was added into the solution and mixed immediately. After the reaction, the black reduced graphene oxide (rGO) hydrogel was obtained first, then taken out and washed carefully with deionized water until pH = 7, and finally freeze-dried hydrogel under a vacuum for at least 48 h for future use. The obtained aerogel composite was shortly named the 4-AAG composite.

2.3. Characterization of the 4-AAG Composite

Fourier transform infrared (FT-IR) spectra of the 4-AAG composites and GO were recorded by using an IR Prestige-21 spectrometer (Shimadzu, Japan). The surface charge properties of the composite in B-R buffer aqueous solution were easured by a Nano-ZS90 Zetasizer (Malvern, UK). The surface morphologies of the 4-AAG composite were recorded under an Ultra Plus scanning electron microscope (SEM, Zeiss, Jena, Thuringia, Germany), in which Schottky field emission electron sources were used. X-ray photoelectron spectroscopy (XPS) scanning curves of the 4-AAG composite were obtained on an ESCALAB 250 spectrometer (Thermo Fisher, Waltham, MA, USA). Raman spectra of the 4-AAG composite were recorded on a Laser Raman spectroscopy (LabRAM XploRA, Paris, France) with a 638 nm excitation laser.

2.4. Pt (IV) Adsorption and Desorption Process

As a solid adsorbent, 1.0 mg of the 4-AAG composite was mixed into 1.0 mL of Pt (IV) chloride acid solution (the original concentrations were all 80.0 μg·mL^{-1}) varied pH from 3 - 12 by B-R buffer in a 1.5 mL centrifuge tube. Afterward, the centrifuge tube was mixed for a while, then incubated for a few minutes. Finally, the phase separation was performed via centrifugation. The surfactant, urea and B-R buffer were used as eluent reagents to recover Pt (IV) retained on the 4-AAG composite in the desorption experiment. Thereafter, the supernatant (the residual Pt (IV)) was determined by atomic absorption spectrometer (AAS) AA-6300 (Shimadzu, Japan).

3. Results and Discussion

3.1. Preparation and Characterization of the 4-AAG Composite

The FT-IR spectra of 4-AAG composite and GO showed that GO was reduced

into rGO (Figure 1). Comparing the FT-IR spectrum of GO, the adsorption band of C=O stretching vibration at 1631.48 cm^{-1} (Figure 1a) was moved to 1717.70 cm^{-1} and the intensity of C=O was weaker due to the redox reaction of the -C=O on the structure of GO partly happened and the amounts of oxygen-containing groups reduced [24] [28]. It illustrated that part carbonyl groups were preserved in the structure of the obtained 4-AAG composite after the reduction reaction. New adsorption bands of -S=O stretching vibration at 1056.34 cm^{-1}, O=S=O stretching vibration at 1376.20 cm^{-1} and 1259.52 cm^{-1}, S-H stretching vibration at 2364.64 cm^{-1} were observed in the spectrum of 4-AAG composite. Besides, the adsorption band of -NH$_2$ out of plane bending vibration at 876.78 cm^{-1} appeared. It demonstrated that parts of sulphone groups on the structure of the 4-amino-benzenesulfonic acid were reduced into -S=O or -SH, resulting in sulfuryl, sulfhydryl and sulfoxide groups being functionalized on the structure of the obtained aerogel. Furthermore, amino groups from the EDA which uninvolved in the reaction were modified on the 4-AAG composite successfully.

The variation elemental composition of the 4-AAG composite was determined by X-ray photoelectron spectrum (XPS) (Figure 2a), the peaks at 164.84, 284.81, 399.82 and 531.71 eV respectively attributed to the sulfur, carbon, nitrogen and oxygen element. Comparing the XPS spectrum of GO [28], the intensity of the carbon element was increased because of the decrease of the oxygen-containing functional groups, and two new peaks of sulfur element and nitrogen element appeared. The changes indicated that oxygen was substituted by sulfur from 4-amino-benzenesulfonic acid and nitrogen from ethylenediamine. Besides, the characteristics of sulfur were inserted into Figure 2a, which were the peaks at 164.95 eV and 159.6 eV respectively assigned to S2p$_{1/2}$ and S2p$_{3/2}$ in the spectrum of S2p for the 4-AAG composite. It illustrated that GO was reduced and modified by EDA and 4-amino-benzenesulfonate, which was consistent with the results of the FT-IR spectrum of the 4-AAG composite (Figure 1a).

Both Raman spectra of GO and 4-AAG composite had two intense D band and G band (Figure 2b), in which D band corresponds to the breathing mode of aromatic rings with dangling bonds and G band is associated with the bond stretching of sp^2 carbon pairs, which belongs to the feature peaks of graphene [29]. The D/G intensity ratio of the GO composite was 0.993, while the corresponding ratio of the 4-AAG composite was 1.05. After the reaction process, the D/G intensity ratio increased from 0.993 to 1.05, which was consistent with previous papers [30] [31] [32] [33]. It meant GO was reduced into a 4-AAG composite successfully.

The SEM images of GO and 4-AAG composite were characterized by the scanning electron microscope (Figure 3). As shown in Figure 3a, van der Waals force or conjugate interaction drove GO sheets adhere or stack together to form mono block [34] [35] [36]. After the reaction, the stacking sheets became thinner than GO sheets and the wrinkles distribution is much clear. The sizes of holes

distributed randomly in the internal structure. A material that is under the action of high temperatures is influenced by a heat flow which will involve a temperature distribution [37] [38], resulting the different pore-diameters. It illustrated that a three-dimensional foam-like structure was forming after GO in situ self-assembly under atmospheric pressure.
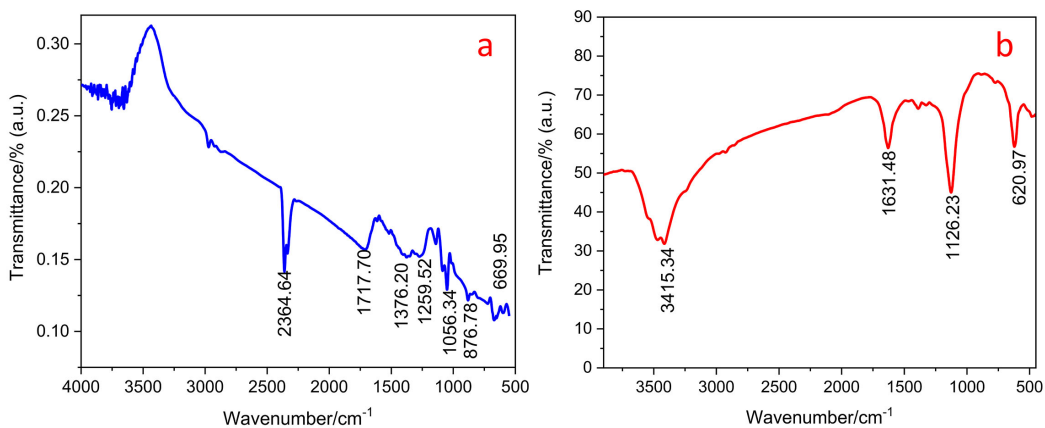
Figure 1. FT-IR spectra of 4-AAG composite (a) and GO (b).
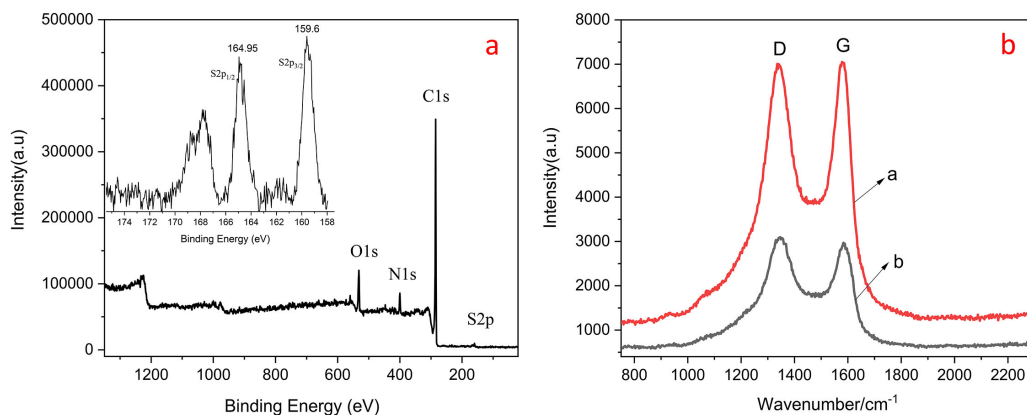
Figure 2. X-ray photoelectron spectrum of the 4-AAG composite (a). Insert a narrow scan of sulfur element. Raman spectra (b) of GO (a) and 4-AAG composite (b).
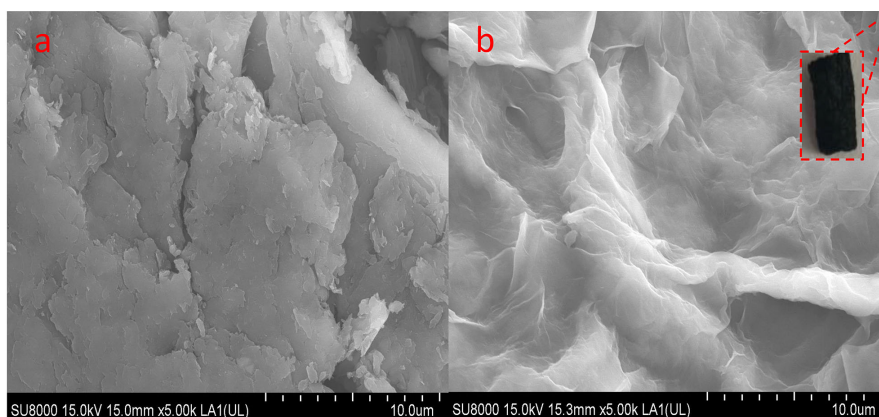
Figure 3. SEM images of GO (a) and 4-AAG composite (b).

3.2. Pt (IV) Adsorption/Desorption Experiment

The adsorption behavior of Pt (IV) on the surface of the 4-AAG composite was performed in a 4 mM B-R buffer where pH varied from 3 - 12 (Figure 4). The good adsorption rate of Pt (IV) was obtained in the acidic condition, while the increase of pH resulted in a decrease in adsorption efficiency (Figure 4a). In industrial production, Pd (II) was one of the main interferences in separating Pt (IV) by liquid-liquid solvent extraction. It was very difficult to isolate Pt (IV) from Pd (II) and Pt (IV) mixture of acidic aquatic solution because of their similar properties. Then we used palladium (II) chloride as a model to investigate the adsorption behavior on the surface of the composite as illustrated in Figure 4b. The 4-AAG composite exhibited a weaker adsorption affinity to Pd (II) under pH 3 - 7, giving a rising of adsorption rate < 50%. For further understanding the adsorption process of Pt (IV), we explored the effect of time on the adsorption efficiency of the 4-AAG composite at pH 6 (Figure 4d). The adsorption efficiency increased with the addition of time, while the adsorption efficiency slightly descended to ~80% after 40 mins. As shown in Figure 4c, the 4-AAG composite charged negativly ranging from pH 4 - 12, electrostatic attraction can drive Pt (IV) ions to adsorb onto the composite.

The desorption experiment was performed to understand the adsorption mechanisms further, we used SDS, TBAB, B-R buffer and deionized water as eluents to replace Pt (IV) from the surface of the composite as illustrated in Figure 5. All of them only can elute less part of Pt (IV), giving a recovery of Pt (IV) of 43.42 %, 12.45 % and 41.85 % respectively attributed to 0.5% SDS, 0.5% TBAB and pH 9 B-R buffer. Moreover, CTAB and urea were used in Pt (IV) and Pd (II) desorption experiments as shown in Figure 6. While the desorption rate of Pt (IV) was effectively improved to 53.96% and 81.13% due to the using 1% urea and 2% CTAB, respectively. Urea was used as an eluent as one of the methods to prove the existing of hydrogen bonds, which had been reported in papers [39] [40] [41]. Urea can displace Pt (IV) from the surface of the composite, meaning that hydrogen bond interaction plays an important role in the adsorption process (Figure 5b). As shown in Figure 6a, the desorption rate ups end with the amount of CTAB added. However, the concentration of CTAB > 2%, was difficult to dissolve and the solution was turbid easily, which influenced determinate results. The recovery rate of Pt (IV) was >66% while the concentration of CTAB was >1.5%. CTAB is a commonly used cationic surfactant. CTAB competed with Pt (IV) ions to adsorb on the negatively charged surface of the 4-AAG composite. It proved that electrostatic interactions have mainly driven Pt (IV) adsorb onto the composite. Although TBAB was cationic surfactant and had branched chains, which were shorter than CTAB. Compared with TBAB (Figure 5b), CTAB had a long hydrophobic chain, and might easily displace Pt (IV) by van der Waals force.

From Figure 4b, the 4-AAG composite showed unfavorable for Pd (II) under acidic conditions. Therefore, the desorption experiment of Pd (II) was per-

formed by using urea (**Figure 6d**) and CTAB (**Figure 6c**) as eluents. The recovery of Pd (II) was 74.56% by using 0.5% CTAB, however, the desorption rate decreased as the adding of concentration of CTAB. Besides, 0.5% urea was added to desorb the adsorbed Pd (II), giving a rise to the recovery of 69.17%. Only a few Pd (II) were eluted with the increase in the amount of urea. Thus, it is possible to remove Pd (II) by elution process when the Pt (IV) solution mixes partly with Pd (II) after the adsorption experiment at acid condition.
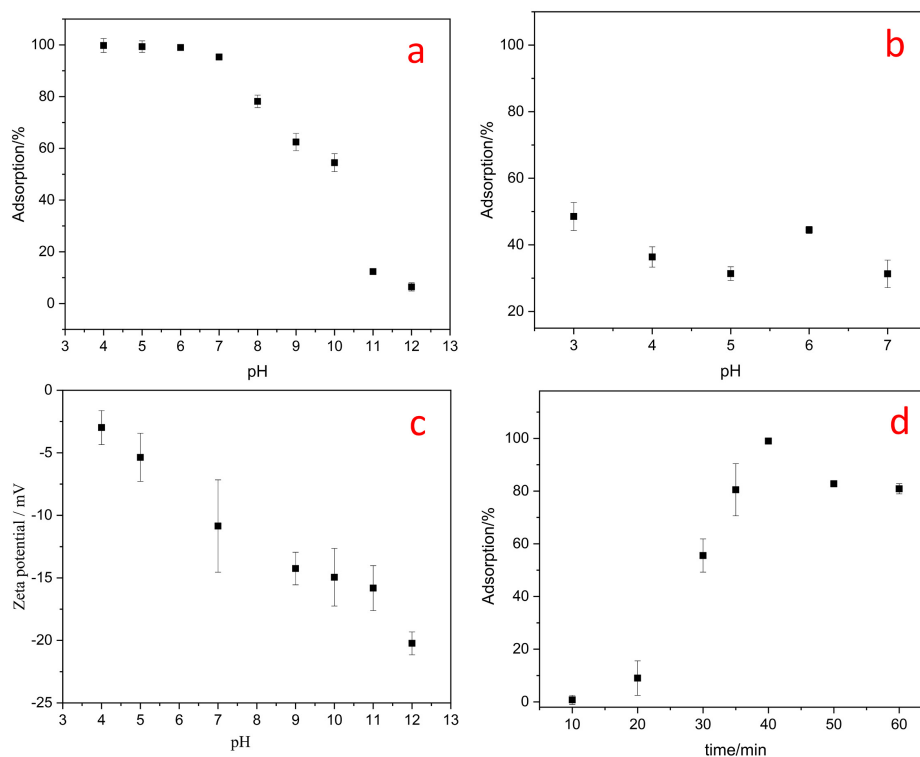
Figure 4. pH-dependent adsorption efficiencies of Pt (IV) (a) and Pd (II) (b) onto the 4-AAG composite with adsorption time of 30 mins; ζpotential of the 4-AAG composite dispensed in 40 mM B-R buffer from pH 4 - 12 (c); effect of time on the adsorption efficiency of the 4-AAG composite for Pt (IV) (d). Concentration/volume of each solution, 80 μg·mL^{-1}/1.0mL; adsorbent, 1.0 mg.
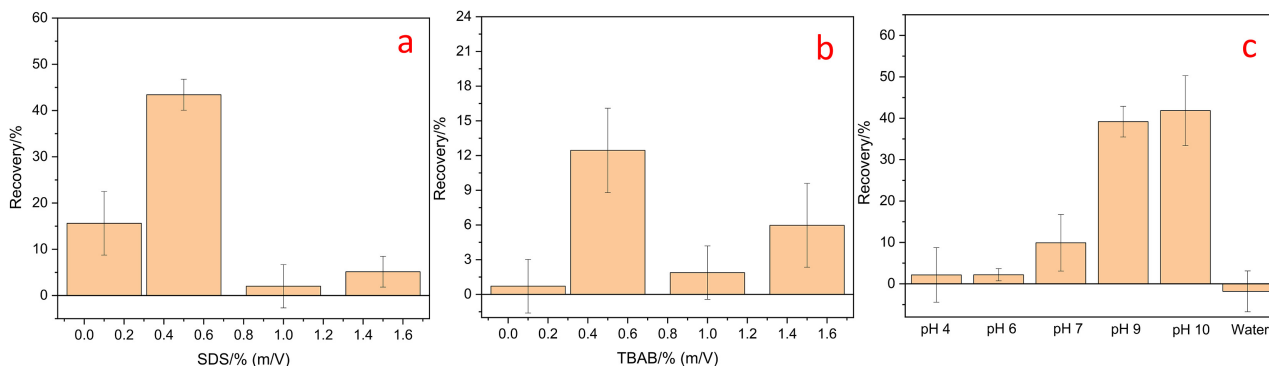
Figure 5. The effect of the amount of SDS (a), TBAB (b) and B-R buffer (c) on the recovery of Pt (IV). Adsorbent, 1.0 mg; volume, 1.0 mL; time, 40 min.
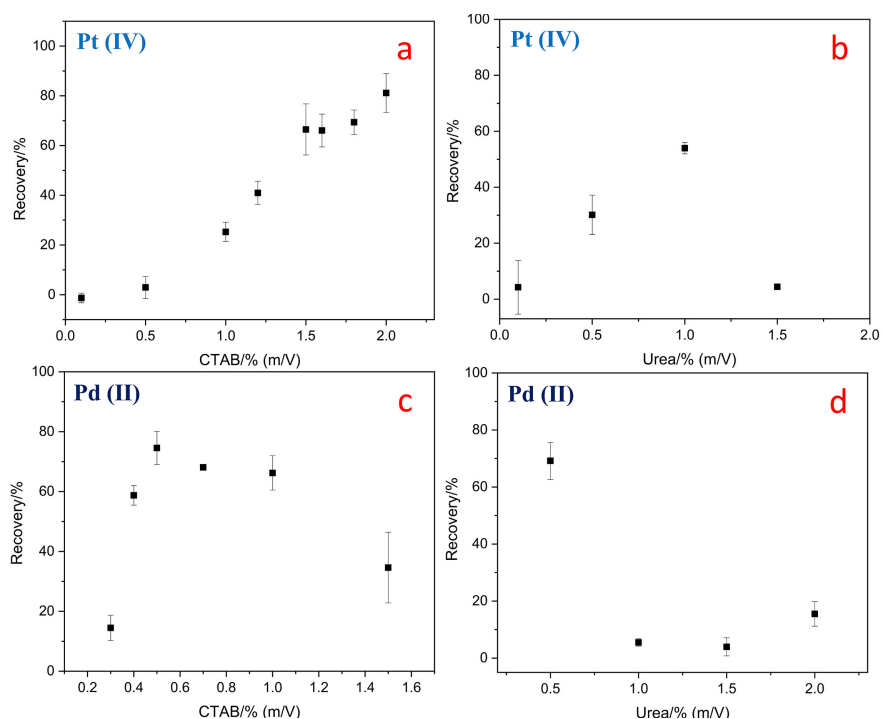
Figure 6. The effect of the amount of CTAB (a) and urea (b) on the recovery of Pt (IV); the effect of the amount of CTAB (c) and urea (d) on the recovery of Pd (II). Adsorbent, 1.0 mg; volume, 1.0 mL; time, 40 min.

The adsorption capacity of Pt (IV) onto the surface of 4-AAG composite was illustrated in **Figure 7a**. The concentration of Pt (IV) varied from 50 - 200 µg/mL^{-1} with pH 6 and adsorption time was 40 mins, ~115 µg/ mg^{-1} adsorption capacity was obtained. Then, we performed the adsorption and desorption behavior of Pt (IV) onto the two composites, which were 4-AAG composite and three-dimensional aerogel without 4-amino-benzenesulfonic acid. As shown in **Figure 7b**, the adsorption efficiency of Pt (IV) improved obviously by using the modified three-dimensional graphene. Besides, the desorption efficiency of Pt (IV) from 4-AAG composite was better than graphene aerogel without 4-amino-benzenesulfonic acid. It meant that the stronger adsorption happened between the Pt (IV) and graphene aerogel without 4-amino-benzenesulfonic acid, which harm Pt (IV) recycle. The adsorption and desorption efficiency of Pt (IV) can effectively improved as a whole, which is in favor of the enrichment of Pt (IV) at a low concentration.

Finally, to evaluate the enrichment effect of the 4-AAG composite for Pt (IV) at low concentrations, we used the prepared 4-AAG composite to adsorb 80 µg/mL^{-1} Pt (IV) and Pd (II) mixing B-R buffer (pH 6) solution, then eluted by 1 mL of urea and CTAB, respectively. As shown in **Figure 7c**, the adsorption of Pt (IV) was 91.17%, however, the adsorption of Pd (II) added to 61.12%. It was interesting that the existence of Pt (IV) promoted the Pd (II) adsorption process under pH 6, while the Pd (II) ions had almost no influence on the Pt (IV) adsorption in the mixture solution. Therefore, we might use eluents to remove Pd
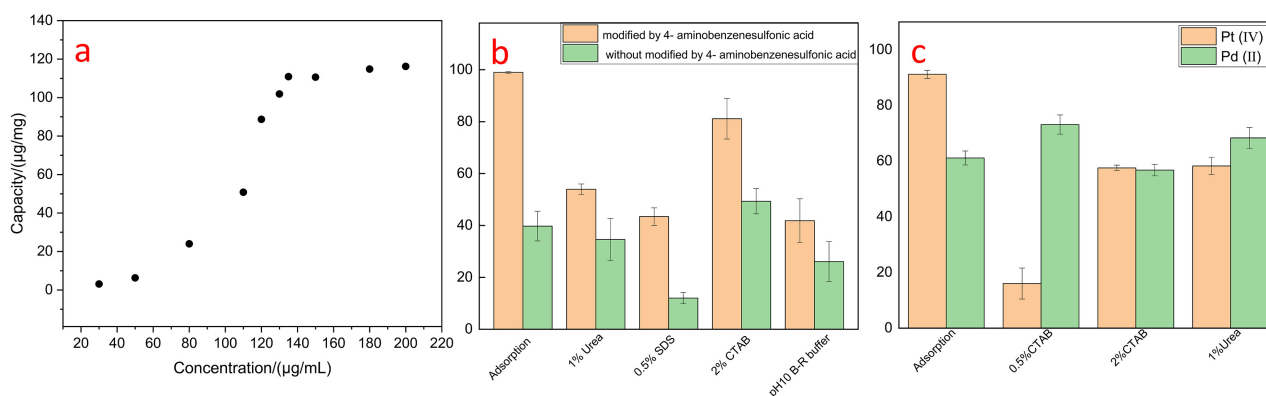
Figure 7. The adsorption capacity of 4-AAG composite for Pt (IV) (a), comparison of the adsorption and recovery of Pt (IV) onto the two composites (b) and comparison of the adsorption and recovery of Pt (IV) and Pd (II) mixing solution (c).

(II) ions interference for enrichment Pt (IV) according to the results of **Figure 6** and **Figure 7c**. Although 2% CTAB and 1% urea showed a similar desorption ability for Pt (IV) and Pd (II) from the surface of 4-AAG composite, 0.5% CTAB can replace 73.15% Pd (II), meanwhile only 16.02% Pt (IV) was eluted. Based on previous research results, it had a big potential for us to use the obtained 4-AAG composite to enrich the Pt (IV) from the mixture solution under acidic conditions, then used 0.5% CTAB to remove the Pd (II) from the Pt (IV) collection.

4. Conclusion

In this work, we used 4-amino-benzenesulfonic acid as sulfur resource and EDA as a crosslinker to prepare the three-dimensional graphene-based composite by a simple method at atmospheric pressure. Then, the separation and enrichment of Pt (IV) by using the 4-AAG composite were performed. Pt (IV) adsorbed onto the composite under the combined action of electrostatic attraction, hydrogen bond interaction and van der Waals force in this process. The composite showed a better affinity for Pt (IV) under acidic conditions, while the adsorption of the composite for Pd (II) was unfavorable enough. The adsorption efficiency of Pd (II) was improved obviously in the Pd (II)/Pt (IV) mixing solution. Moreover, 0.5% CTAB can desorb most of the Pd (II), and only a few Pt (IV) was eluted. It can remove Pd (II) from the Pt (IV) solution further. This research provided a reference surface adsorption interaction between the 4-AAG composite and Pt (IV). A new graphene-based composite was prepared in a simple way. Then it is possible to use this composite to enrich Pt (IV) from a low concentration in a green method, for meeting the requirements of detection limit and low content recovery.

Acknowledgements

Conflicts of Interest

The authors declare no conflicts of interest regarding the publication of this paper.

References

[1] Kraus, P. and Frank, I. (2017) On the Dynamics of H_2 Adsorption on the Pt(111) Surface. *International Journal of Quantum Chemistry*, **117**, e25407. https://doi.org/10.1002/qua.25407

[2] Yao, Y., Yang, Y., Wang, Y., Zhang, H., Tang, H., Zhang, H., Zhang, G., Wang, Y., Zhang, F. and Yan, H. (2021) Photo-Induced Synthesis of Ternary Pt/rGO/COF Photocatalyst with Pt Nanoparticles Precisely Anchored on rGO for Efficient Visible-Light-Driven H_2 Evolution. *Journal of Colloid and Interface Science*, **608**, 2613-2622. https://www.sciencedirect.com/science/article/abs/pii/S0021979721018737

[3] Park, J., Kim, D., Byun, S.W., Shin, H., Ju, Y., Min, H., Kim, Y. J., Heo, I., Hazlett, M. J., Kim, M. and Kang, S.B. (2022) Impact of Pd: Pt Ratio of Pd/Pt Bimetallic Catalyst on CH_4 Oxidation. *Applied Catalysis B*: *Environmental*, **316**, 121623-121632. https://www.sciencedirect.com/science/article/abs/pii/S0926337322005641

[4] Liu, D., Hu, H., Yang, Y., Cui, J., Fan, X., Zhao, Z., Kong, L., Xiao, X. and Xie, Z. (2022) Restructuring Effects of Pt and Fe in Pt/Fe-DMSN Catalysts and Their Enhancement of Propane Dehydrogenation. *Catalysis Today*, **402**, 161-171. https://www.sciencedirect.com/science/article/abs/pii/S0920586122001067

[5] Lee, J., Yoo, J.K., Lee, H., Kim, S.H., Sohn, Y. and Rhee, C.K. (2019) Formic Acid Oxidation on Pt Deposit Model Catalysts on Au: Single-Layered Pt Deposits, Plateau-Type Pt Deposits, and Conical Pt Deposits. *Electrochimica Acta*, **310**, 38-44. https://www.sciencedirect.com/science/article/abs/pii/S0013468619307935

[6] Vikla, A.K.K., Simakova, I., Demidova, Y., Keim, E.G., Calvo, L., Gilarranz, M.A., He, S. and Seshan, K. (2020) Tuning Pt Characteristics on Pt/C Catalyst for Aqueous-Phase Reforming of Biomass-Derived Oxygenates to Bio-H_2. *Applied Catalysis A*: *General*, **610**, Article ID: 117963. https://www.sciencedirect.com/science/article/pii/S0926860X20305561

[7] Peng, Y., Choi, J.Y., Fürstenhaupt, T., Bai, K. and Zhang, Y. (2021) Dustin Banham New Approach for Rapidly Determining Pt Accessibility of Pt/C Fuel Cell Catalysts. *Journal of Materials Chemistry A*, **9**, 13471-13476. https://pubs.rsc.org/en/content/articlelanding/2021/ta/d1ta01769a

[8] Zhao, T., Hu, Y., Gong, M., Lin, R., Deng, S., Lu, Y., Liu, X., Chen, Y., Shen, T., Hu, Y., Han, L., Xin, H., Chen, S. and Wang, D. (2020) Electronic Structure and Oxophilicity Optimization of Mono-layer Pt for Efficient Electrocatalysis. *Nano Energy*, **74**, 104877-104903. https://www.sciencedirect.com/science/article/abs/pii/S2211285520304341

[9] Yang, X., Xing, C., Zhang, B., Liu, X., Liang, H., Luo, G., Zhang, G., Li, Z., Zhao, S., Zhang, J., Wang, G. and Qin, Y. (2022) Direct Bonding of CpCo-Fragments on Pt Nanoparticles and their Electronic Effect for Alkyne Semihydrogenation. *ACS Catalysis*, **12**, 10849-10856. https://pubs.acs.org/doi/abs/10.1021/acscatal.2c03024

[10] Reimers, J.R., Wang, Y. and Kosov, D.S. (2019) Decomposition of Ferrocene on Pt (111) and Its Effect on Molecular Electronic Junctions. *The Journal of Physical Chemistry C*, **123**, 15569-15574. https://doi.org/10.1021/acs.jpcc.9b02628

[11] Anantharaj, S. (2022) Hydrogen Evolution Reaction on Pt and Ru in Alkali with

Volmer-Step Promotors and Electronic Structure Modulators. *Current Opinion in Electrochemistry*, **33**, 100961-100984.
https://www.sciencedirect.com/science/article/abs/pii/S2451910322000266

[12] Malhotra, S., Tang, Y. and Varshney, P.K. (2019) Fabrication of Highly Sensitive Non-Enzymatic Sensor Based on Pt/PVF Modified Pt Electrode for Detection of Glucose. *Journal of the Iranian Chemical Society*, **17**, 521-531.
https://link.springer.com/article/10.1007/s13738-019-01786-0?utm_source=xmol&utm_medium=affiliate&utm_content=meta&utm_campaign=DDCN_1_GL01_metadata

[13] Meng, D., Zhang, S., Thomas, T., Huang, C., Zhao, J., Zhao, R., Shi, Y., Qu, F. and Yang, M. (2020) Pt/WN Based Fuel Cell Type Methanol Sensor. *Sensors and Actuators B: Chemical*, **307**, 127686-127693.
https://www.sciencedirect.com/science/article/abs/pii/S0925400520300332

[14] Zuo, P., Wang, R., Li, F., Wu, F., Xu, G. and Niu, W. (2021) A Trace ppb-Level Electrochemical H_2S Sensor Based on Ultrathin Pt Nanotubes. *Talanta*, **233**, 122539-122544.
https://www.sciencedirect.com/science/article/abs/pii/S0039914021004604

[15] Gao, A., Wu, Y., Yu, J., Gong, H., Jiang, J., Yang, C., Liu, W. and Qing, C. (2022) Synthesis and Anticancer Activity of Two Highly Water-Soluble and Ionic Pt(IV) Complexes as Prodrugs for Pt(II) Anticancer Drugs. *RSC Medicinal Chemistry*, **5**, 594-598. https://pubs.rsc.org/en/content/articlelanding/2022/md/d2md00004k

[16] Rana, U., Chakraborty, C., Kanao, M., Morita, H., Minowa, T. and Higuchi, M. (2019) DNA-Binding, Cytotoxicity and Apoptosis Induction of Pt/Fe-Based Heterometallo-Supramolecular Polymer for Anticancer Drug Application. *Journal of Organometallic Chemistry*, **891**, 28-34.
https://www.sciencedirect.com/science/article/abs/pii/S0022328X19301238

[17] Ma, L., Ma, R., Wang, Z., Yiu, S. and Zhu, G. (2016) Heterodinuclear Pt(IV)-Ru(II) Anticancer Prodrugs to Combat both Drug Resistance and Tumor Metastasis. *Chemical Communications*, **52**, 10735-10738.
https://pubs.rsc.org/en/content/articlelanding/2016/CC/C6CC04354B

[18] Ano, S.O., Intini, F.P., Natile, G. and Marzilli, L.G. (1998) A Novel Head-to-Head Conformer of d (GpG) Cross-linked by Pt: New Light on the Conformation of Such Cross-Links Formed by Pt Anticancer Drugs. *Journal of the American Chemical Society*, **120**, 12017-12022. https://doi.org/10.1021/ja9805674

[19] Demas, J.N. and DeGraff, B.A. (2001) Applications of Luminescent Transition Platinum Group Metal Complexes to Sensor Technology and Molecular Probes. *Coordination Chemistry Reviews*, **211**, 317-351.
https://www.sciencedirect.com/science/article/abs/pii/S0010854500002782?via%3Dihub

[20] Ma, D.L., Che, C.M. and Yan, S.C. (2009) Platinum(II) Complexes with Dipyridophenazine Ligands as Human Telomerase Inhibitors and Luminescent Probes for G-Quadruplex DNA. *Journal of the American Chemical Society*, **131**, 1835-1846.
https://doi.org/10.1021/ja806045x

[21] Zou, T., Liu, J., Lum, C.T., Ma, C., Chan, R.C.T., Lok, C.N., Kwok, W.M. and Che, C.M. (2014) Luminescent Cyclometalated Platinum(II) Complex Forms Emissive Intercalating Adducts with Double-Stranded DNA and RNA: Differential Emissions and Anticancer Activities. *Angewandte Chemie International Edition*, **53**, 10119-10123. https://doi.org/10.1002/anie.201405384

[22] Tang, J., Huang, D., Meng, F., Li, P., Peng, F. and Huang, J. (2020) Novel Platinum

(II) Complex-Based Luminescent Probe for Detection of Hypochlorite in Cancer Cells. *Photochemistry and Photobiology*, **97**, 317-326. https://doi.org/10.1111/php.13344

[23] U.S. Geological Survey (2022) Mineral Commodity Summaries 2022. 126-127. https://pubs.er.usgs.gov/publication/mcs2022

[24] Chen, L., Zheng, D.H., Zhang, Y., Wang, Y.N. and Xu, Z.R. (2017) *In Situ* Self-Assembled Reduced Graphene Oxide Aerogel Embedded with Nickel Oxide Nanoparticles for the High-Efficiency Separation of Ovalbumin. *Journal of Separation Science*, **40**, 1765-1772. https://doi.org/10.1002/jssc.201601322

[25] Liu, B., Xie, J., Ma, H., Zhang, X., Pan, Y., Lv, J., Ge, H., Ren, N., Su, H., Xie, X., Huang, L. and Huang, W. (2017) Graphene: From Graphite to Graphene Oxide and Graphene Oxide Quantum Dots. *Small*, **13**, 1601001-1601008. https://doi.org/10.1002/smll.201601001

[26] Liu, S., Cerruti, M. and Barthelat, F. (2020) Plastic Forming of Graphene Oxide Membranes into 3D Structures. *ACS Nano*, **14**, 15936-15943. https://doi.org/10.1021/acsnano.0c07344

[27] Choi, G.M., Park, M., Shim, Y.H., Kim, S.Y. and Lee, H.S. (2021) Mass Production of 2D Manifolds of Graphene Oxide by Shear Flow. *Advanced Functional Materials*, **32**, 2107694-2107703. https://doi.org/10.1002/adfm.202107694

[28] Chen, L. and Xu, Z.R. (2016) A Three-Dimensional Nickel-Doped Reduced Graphene Oxide Composite for Selective Separation of Hemoglobin with a High Adsorption Capacity. *RSC Advances*, **6**, 56278-56286. https://pubs.rsc.org/en/content/articlelanding/2016/ra/c6ra08933j

[29] Kawashima, Y. and Katagiri, G. (1995) Fundamentals, Overtones, and Combinations in the Raman Spectrum of Graphite. *Physical Review B*, **52**, 10053-10061. https://journals.aps.org/prb/abstract/10.1103/PhysRevB.52.10053

[30] Cheng, J., Li, Y., Huang, X., Wang, Q., Meib, A. and Shen, P.K. (2015) Highly Stable Electrocatalysts Supported on Nitrogen-Self-Doped Three-Dimensional Graphene-Like Networks with Hierarchical Porous Structures. *Journal of Materials Chemistry A*, **3**, 1492-1497. https://pubs.rsc.org/en/content/articlelanding/2015/ta/c4ta05552g

[31] Cao, Y., Chai, D., Luo, Z., Jiang, M., Xu, W., Xiong, C., Li, S., Liu, H. and Fang, D. (2017) Lithium Vanadate Nanowires @ Reduced Graphene Oxide Nanocomposites on Titanium Foil with Super High Capacities for Lithium-Ion Batteries. *Journal of Colloid and Interface Science*, **498**, 210-216. https://www.sciencedirect.com/science/article/abs/pii/S0021979717302436?via%3Dihub

[32] Chi, C., Xu, H., Zhang, K., Wang, Y., Zhang, S., Liu, X., Liu, X., Zhao, J. and Li, Y. (2015) 3D Hierarchical Porous Graphene Aerogels for Highly Improved Adsorption and Recycled Capacity. *Materials Science and Engineering: B*, **194**, 62-67. https://www.sciencedirect.com/science/article/abs/pii/S0921510714003043

[33] Zhao, M., Deng, C. and Zhang, X. (2013) Synthesis of Polydopamine-Coated Magnetic Graphene for Cu^{2+} Immobilization and Application to the Enrichment of Low-Concentration Peptides for Mass Spectrometry Analysis. *ACS Applied Materials & Interface*, **5**, 13104-13112. https://doi.org/10.1021/am4041042

[34] Wang, Y., Li, Z., Wang, J., Li, J. and Lin, Y. (2011) Graphene and Graphene Oxide: Biofunctionalization and Applications in Biotechnology. *Trends in Biotechnology*, **29**, 205-212. https://linkinghub.elsevier.com/retrieve/pii/S0167779911000199

[35] Stankovich, S., Dikin, D.A., Dommett, G.H., Kohlhaas, K.M., Zimney, E.J., Stach,

E.A., Piner, R.D., Nguyen, S.T. and Ruoff, R.S. (2006) Graphene-Based Composite Materials. *Nature*, **442**, 282-286. https://www.nature.com/articles/nature04969

[36] De La Cruz, F. and Cowley, J.M. (1962) Structure of Graphitic Oxide. *Nature*, **196**, 468-469. https://www.nature.com/articles/196468a0#citeas

[37] (1996) Generalized Solutions in Elasticity of Micropolar Bodies with Voids. *Revista de la Academia Canaria de Ciencias*, **8**, 101-106.

[38] (1998) Contributions on Uniqueness in Thermoelastodynamics on Bodies with Voids. *Ciencias matemáticas* (*Havana*), **16**, 101-109.

[39] Wang, Z., Zhou, X., Han, J., Xie, G. and Liu, J. (2022) DNA Coated CoZn-ZIF Metal-Organic Frameworks for Fluorescent Sensing Guanosine Triphosphate and Discrimination of Nucleoside Triphosphates. *Analytica Chimica Acta*, **1207**, 339806-339814. https://www.sciencedirect.com/science/article/abs/pii/S0003267022003774

[40] Zandieh, M., Patel, K. and Liu, J. (2022) Adsorption of Linear and Spherical DNA Oligonucleotides onto Microplastics. *Langmuir*, **38**, 1915-1922. https://doi.org/10.1021/acs.langmuir.1c03190

[41] Wang, J., Wang, Z., Huang, P.J.J., Bai, F. and Liu, J. (2022) Adsorption of DNA Oligonucleotides by Self-Assembled Metalloporphyrin Nanomaterials. *Langmuir*, **38**, 3553-3560. https://doi.org/10.1021/acs.langmuir.2c00108